Use of the simultaneous seismic, GPS and meteorological monitoring for the characterization of a large unstable mountain slope in the southern French Alps

Stéphane Gaffet,[1] Yves Guglielmi,[2] Frédéric Cappa,[1] Claude Pambrun,[1,*] Tony Monfret[1] and David Amitrano[3]

[1]*GEOAZUR (UMR 6526 UNS/CNRS/IRD/OCA), 250, rue Albert Einstein, Sophia-Antipolis,* 06560 *Valbonne, France. E-mail: Stephane.Gaffet@oca.eu*
[2]*GSRC, University of Provence Aix-Marseille* 1, 3 *place Victor Hugo,* 13331 *Marseille, France*
[3]*LGIT* (UMR 5559), 1381 *rue de la piscine,* BP 53, 38041 *Grenoble* Cedex 9*, France*

SUMMARY

The presence of unstable rock slopes in the mountainous regions makes these areas particularly prone to the development of sudden dramatic events, which may cause damage and injuries. The efficient disaster management requires a good understanding of the main causes of these mass movements, such as, increased fluid pressure and seismic shaking. In order to improve our understanding of the mechanics and dynamics of the mountain slope instabilities, we developed a monitoring system based on microseismic, geodetic and meteorological measurements. The system operated in the La Clapière rockslide in the southern French Alps. It was composed of four three-component seismological stations, four Global Positioning Systems (GPS) and three meteorological stations deployed together for a period of 4 months. This system was installed over the territory of $\sim$1.5 km^2 of the fractured gneissic terrain that moves at a mean velocity of about 70 cm yr^{-1}. This passive measurement method may represent an interesting approach to the characterization of the landslides difficult to access, since it allows the use of the lighter instrumentation and easier processing tools. Our investigations were based on the H/V method to image shear wave contrasts that we correlated with slip surfaces. The analysis of the seismograms allowed us to point out a correlation between the thickness of the surface layers and the measured resonance frequencies. The results indicated that the H/V ratios are heterogeneous in the rockslide. Comparison between seismic and GPS data proved our monitoring approach to be promising for landslides characterization.

Key words: Spatial analysis; Geomechanics; Seismicity and tectonics; Surface waves and free oscillations; Site effects.

GJI Seismology

1 INTRODUCTION

Due to the increase in exceptional climatic events, rapid population expansion, land use and growing transportation demands in the mountainous regions the understanding of the risks associated with unstable rock slopes becomes crucially important (Geertsema *et al.* 2006). To efficiently mitigate the effects of rock slope failures, a good understanding of the characteristics of these mass movements is required. It is well known that a mountain slope failure results from the progressive spreading of local failures on pre-existing discontinuities and in intact rock between discontinuities (Scavia 1995; Kemeny 2003; Eberhardt *et al.* 2005). Among the numerous factors that govern the stability of rock slopes, mainly three are usually described (Finlayson & Statham 1980; Noverraz *et al.* 1998).

(1) Seismic shaking of the slope.
(2) Groundwater effects.
(3) Modification of the slope topography: natural (glacial or flood erosion) or artificial (excavation at the foot of the slope).

The processes of earthquakes-induced landslides are well documented in the cases of high-magnitude seismic events (Wilson & Keefer 1983; Jibson & Keefer 1992, 1993; Khazai & Sitar 2004). In such cases, it clearly appears that the epicentral distance and the ground acceleration are the predominant triggering factors. In seismically active areas, the problem can be addressed through more or less complex

*Deceased 2010 February.

1

statistical approaches using for example the Newmark method (Jibson *et al.* 1998). In areas of low-magnitude earthquakes or low-seismicity, slope failure processes are less clear because they depend on many superimposed factors. It is commonly observed that rock slopes have stood in relatively stable conditions over periods of several thousand years until failure occurs (Eberhardt *et al.* 2004; Eberhardt *et al.* 2005). To explain progressive slope failure a component of strength degradation with time must be taken into consideration. Thus, repeated rainfall infiltration and low-frequency seismic shakings caused by distant large magnitude earthquakes can contribute to this progressive strength degradation. Currently, this approach is seldom studied mainly because it requires a long-term multiparametric monitoring. Generally, large landslides are studied using geomorphological and geological observations combined with geotechnical investigations (Glade 2005). In addition to these techniques, geophysical methods were also used to obtain images with a high-resolution of the internal structure of landslides (Jongmans *et al.* 2000; Meric *et al.* 2005; Heincke *et al.* 2006; Jongmans & Garambois 2007; Spillman *et al.* 2007a). Recent studies of the seismic activity of unstable slopes allowed to obtain new information on their mechanism (Del Gaudio & Wasowski 2007; Meric *et al.* 2007; Spillman *et al.* 2007b; Deparis *et al.* 2008).

In this paper, we present the results of a multiparametric monitoring of the La Clapière rockslide in the French Alps. This large mountain slope movement has been extensively studied for the past several years. Following the preliminary seismic studies done in 2001–2002 (CETE 2002a, b), a geophysical and geodetic monitoring system composed of the seismic, GPS and rainfall sensors was installed on the rockslide ground surface for a period from 2003 July to mid-November. Data recorded with this experimental device and introduced herein allowed us to characterize:

(1) the landslide reactions to distant earthquake events,
(2) the most relevant multiparametric measurement array for a long period monitoring that should be set for a continuous survey.

Our approach is based on two types of the analysis:

(1) Spectral H/V analysis in order to determine resonance frequencies and thus identify different rockslide behaviours related to the atmospheric events.
(2) Site to reference analysis of relative ground shaking amplification during earthquake.

After briefly introducing the geology of the study site, we describe our approach to the rockslide monitoring. Then we present an integrated interpretation of the rockslide behaviour based on the analysis of seismic, displacement, and rainfall data.

2 THE LA CLAPIÈRE STUDY SITE: GEOLOGY AND FAULT/FRACTURE SYSTEMS IN AND AROUND THE ROCKSLIDE

The La Clapière unstable slope is located in the Tinée valley at the northwestern edge of the Mercantour External Crystalline Massif in the Southern French Alps (Fig. 1). The current rockslide body whose volume is about 60×10^6 m^3 was triggered in 1951 and, since that date has remained active. Rockslide surface displacements as well as rainfalls are monitored by the French Ministry of Equipment that is also in charge of the management of the risk posed by this rockslide to the valley which is connected to the city of Nice. In 2002 the GeoAzur Laboratory and the Ministry of Equipment started a research collaboration venture in aim to transform this site into a permanent observatory dedicated to the improvement of the knowledge of failure processes in large fractured rock slopes. Many national and European programs have been conducted on the site for more than ten years and its geology, hydrogeology, mechanical properties and active deformation are well characterized (Gunzburger & Laumonier 2002; Guglielmi *et al.* 2002, 2005; Cappa *et al.* 2004).

The East side of the Tinée valley is composed of the metamorphic basement (Guglielmi & Cappa, 2010). The foliation planes are, in average, N150°E oriented dipping to the East with an angle of 60°. Close to the slope surface, within a 100-m-thick shallow zone, foliation is dipping gently (less than 20°) either to the NE or to the SW. Metamorphic rocks are weathered to the depth ranging from 50 to 200 m depending on the zones of the valley. Three sets of faults can be distinguished, trending N010°E–N030°E, N080°E–N090°E and N110°E–N140°E with a dip angle close to 90° (Fig. 1). The rocks located in the upper and middle portions of the slope correspond to two metamorphic facies: (1) a low-altered meta-granodiorite layer (called 'Iglière bar' and coloured in grey on Fig. 1), which is embedded in (2) two-mica gneisses that are highly altered from the topographic surface to the depth of 100 m in the slope (Cappa *et al.* 2004; Guglielmi *et al.* 2005). The top of the La Clapière rockslide corresponds to a 120 m high scarp that extends over a width of 800 m at the elevation of 1600 m. The depth of the failure surface varies between 80 and 100 m from the topographic surface (Fig. 1). The rockslide body is highly fractured and can be schematically divided into four zones (Cappa *et al.* 2004).

(1) The two main central volumes that are located at the elevation between 1100 m and 1600 and separated by a major scarp. The scarp is oriented N90°E and is dipping 50° towards the valley. These two volumes are made up of fractured rocks moving downward at a velocity from 45 to 90 cm/yr depending on the season.
(2) The upper north-eastern compartment (estimated volume of 5×10^6 m^3) that behaves like an isolated block sliding along its own failure surface and overlapping the main rockslide at a velocity varying between 100 and 380 cm yr^{-1}.
(3) The upper northwestern compartment which is limited to the South by a 150 m high scarp of the main landslide failure surface, and to the North by a 50 m high scarp. This compartment behaves like a fractured rock mass with active tension cracks and velocities ranging between 20 and 70 cm yr^{-1}.
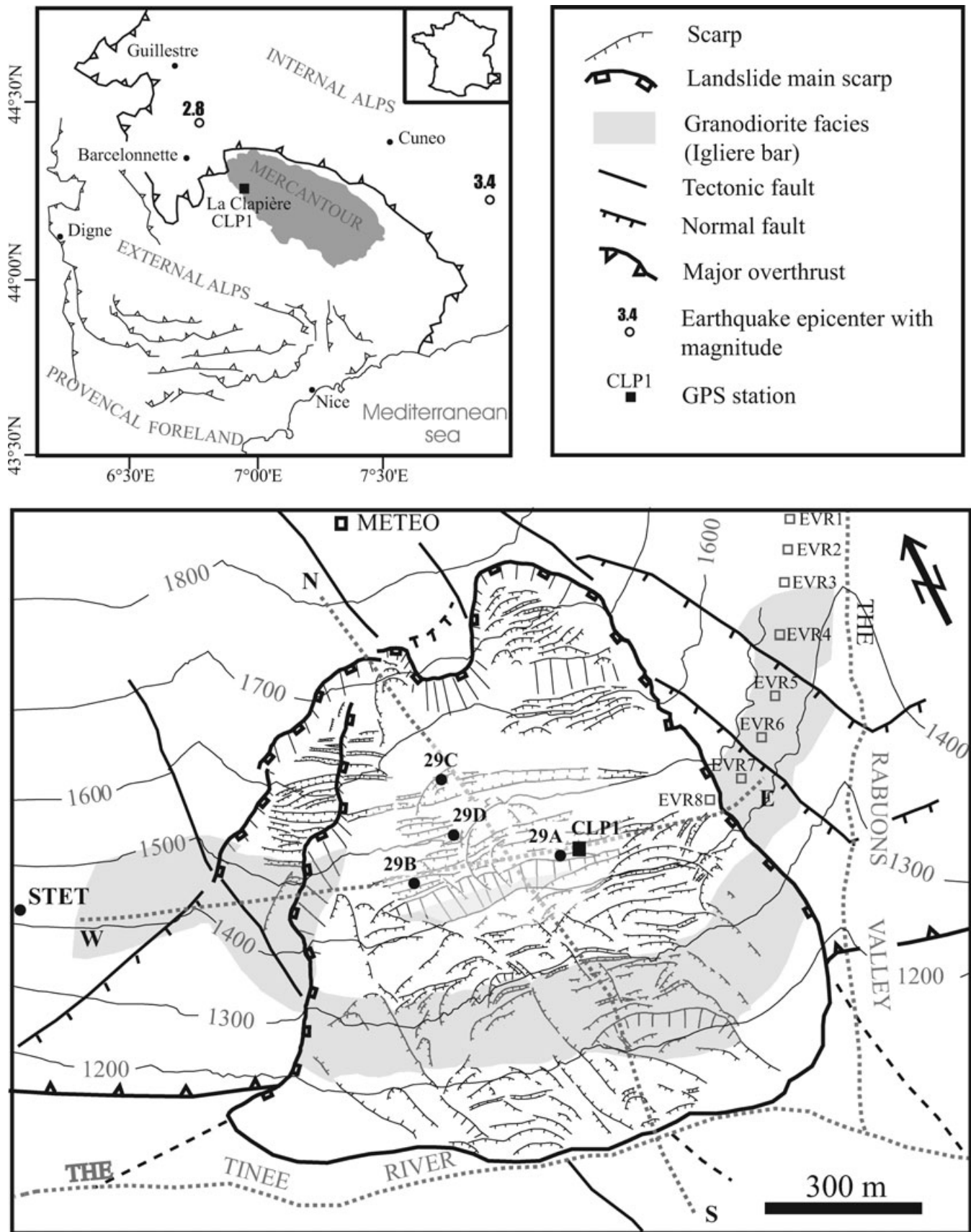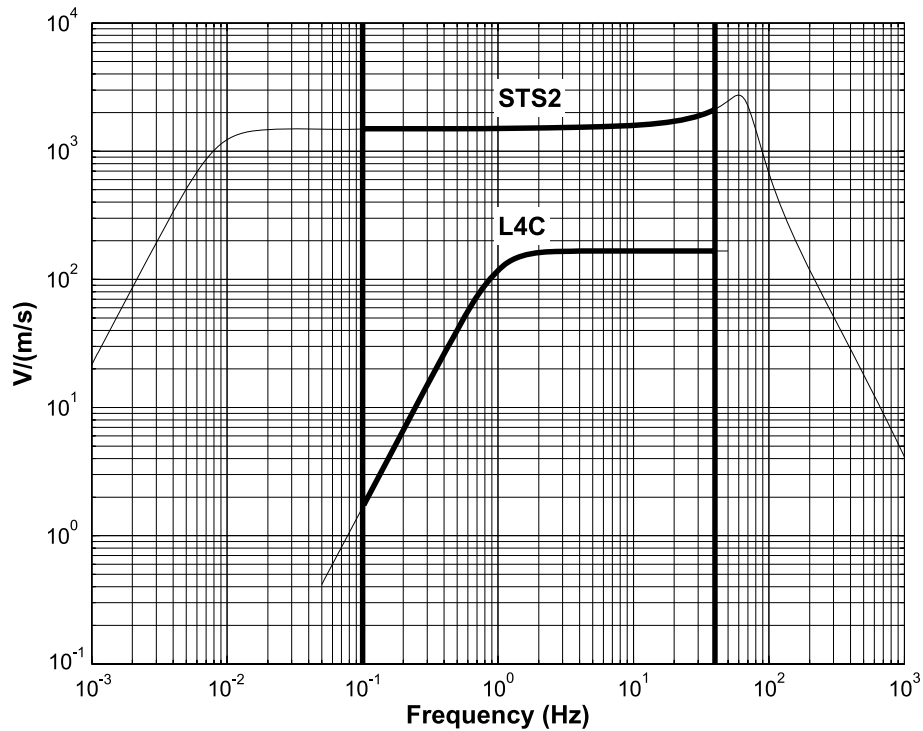
Figure 1. Top map: location of the La Clapière landslide on the western part of the Argentera Mercantour massif. Bottom map: detailed structural map of the landslide with the seismometric array.

Figure 2. Amplitude response of the seismometers to ground velocity. Flat level corresponds to 1500 V (m s^{-1})$^{-1}$ for the STS2 sensor located at the reference site 'STET', and 166 V (m s^{-1})$^{-1}$ for the L4C (Bowden, 2003) sensors on the rockslide. The common frequency range is denoted by the thick bold line between 0.1 and 40 Hz.

3 THE LA CLAPIÈRE ROCKSLIDE: A PERMANENT OBSERVATORY WITH A MONITORING SYSTEM BASED ON A NETWORK OF SEISMIC, GEODETIC AND METEOROLOGICAL SENSORS

Four Mark Product L4C triaxial short period inertia passive seismometers were installed on the rockslide at the locations 29A, 29B, 29C and 29D (Fig. 1). In addition, a Streckeisen STS2 broad-band seismometer (STET) provided by the RENASS network (http://renass.u-strasbg.fr/) was settled on the stable rock basement, 1 km eastward of the rockslide (Fig. 1). The four stations on the rockslide were located on the independent soil slumps corresponding to the original soil layer which slid along the rockslide while preserving its structure. Station 29C was located above slid gneiss under the main 120 m high head scarp upper limit of the actual landslide.

The short period network was installed on the main central rockslide volume behind the upper northeastern overlapping compartment and the upper northwestern fractured but actually probably not sliding compartment (Guglielmi *et al.* 2005). The seismometers were settled on the buried concrete basements with a maximum distance of 200 m between each other. Sensitivities and frequency ranges of these seismometers of two kinds are displayed in Fig. 2. Ground velocity was recorded in a continuous mode by 24 bits Agecodagis digitizers with a 125 pts s^{-1} sampling rate. Time was controlled by Leas GPS antennas. Solar panels connected to three batteries per site provided energy to the digitizers and GPS clock.

In addition to this seismic network, a Near Real-Time GPS survey system was developed in and around the rockslide (Fig. 1). Two bi-frequency GPS (Ashtech Mira-Ze) were installed in the stable areas surrounding the rockslide, and were used as no moving reference sites. Two single-frequency GPS receivers (Ashtech G12) and antenna were installed within the sliding area. CLP1 was located in a fast sliding area which served as a good representative of the dynamics of the main part of the rockslide (Fig. 1). The second site CLP2 was installed at the edge of the main rockslide area on an intermediate block between the main sliding area and the stable area.

We also developed a meteorological measurement system to quantify the daily amount of water precipitated in the slope. These measurements were done with the help of the rain and snow gauges located at the foot of the slope (1100 m elevation), in the middle of the slope (1800 m elevation) and at the top of the slope (2500 m elevation).

4 SEISMIC RECORD ANALYSIS

In this part, we present the method that we employed to characterize the rockslide by using the data of the analysis of the recorded seismograms.

4.1 H/V method

The H/V method involves computing the spectral ratio between the horizontal and vertical components of the seismic noise recorded simultaneously at a given location with the 3-D seismometer placed at the ground surface. This method is commonly used to estimate the seismic response of the surface layers (Nogoshi & Igarashi 1970).

In our study, for each station, the whole data set (140 d) is split in 1-hr sections (Fig. 3) in order to process H/V analysis (Nogoshi & Igarashi 1970; Nakamura 1989, 2000). The aim of this analysis is to identify potential resonance frequencies and their variations. The Nakamura's technique (Nakamura 1989) initially developed to produce a fast investigation of site effects related to unconsolidated soils (e.g. colluviums, alluviums) is based on three main hypotheses: (1) the ambient noise is generated by surface waves and multiply reflected and refracted shear waves trapped in the considered soil, (2) the sources of noise at the surface do not influence the noise at the bottom of the soil and (3) any vertical amplification of noise at the surface can be associated with propagation effects within the soil itself. Under these assumptions, the characterization of the site response may be represented by the spectral ratio of the vertical to horizontal components of the noise recorded at the surface. This spectral ratio allows identification of the resonance frequencies f. Each resonance frequency is related to the depth H of the soil bottom by the equation $f = \beta/(4H)$, where β is the mean shear velocity of the medium between the surface and the related bottom interface.

The H/V analysis is processed hereunder for all elementary windows with length $T \approx 130$ s (i.e. 2^{14} points) moving along each 1-hr section with step $S \approx T/2$ s (i.e. 2^{13} points). This process leads to approximately 120 realizations for each 1-hr section (Fig. 4). The elementary window length T allows by itself a good statistical representation of all periods of interest between 1 and 0.025 s (40 Hz). Each window is mean value removed, detrended and windowed prior to calculations.

For each 1-hr window section at station i and for each related elementary time window m, the spectral ratio $r_{i,n}(f)$ of Fourier spectra is computed as follows:

$$r_{i,m}(f) = L_w \left(\frac{\sqrt{|FFT(n_{i,m}(t))|^2 + |FFT(e_{i,m}(t))|^2}}{|FFT(z_{i,m}(t))| + \varepsilon} \right), \quad \text{with } \varepsilon = \max(|FFT(z_{i,m}(t))|)/20 \tag{1}$$

where $z_{i,m}(t)$, $n_{i,m}(t)$ and $e_{i,m}(t)$ denote the vertical, north-south, and east-west components of the ground motion analysed. The factor ε is added to the denominator spectrum in order to avoid possible over amplifications generated by small energetic or noisy frequency band of the denominator (Mari *et al.* 1997). The value 20 used to compute ε has been adopted experimentally because it is well adapted to preserve the amplitude of the calculated ratios inside the energetic frequency bands, and it allows the ratio to drop down at frequencies where the seismic energy is vanishing (Gaffet *et al.* 2000). The function L_w is a smoothing window with w Hz half width centred onto frequency f, length of the triangular smoothing function used being w = 0.35 Hz.
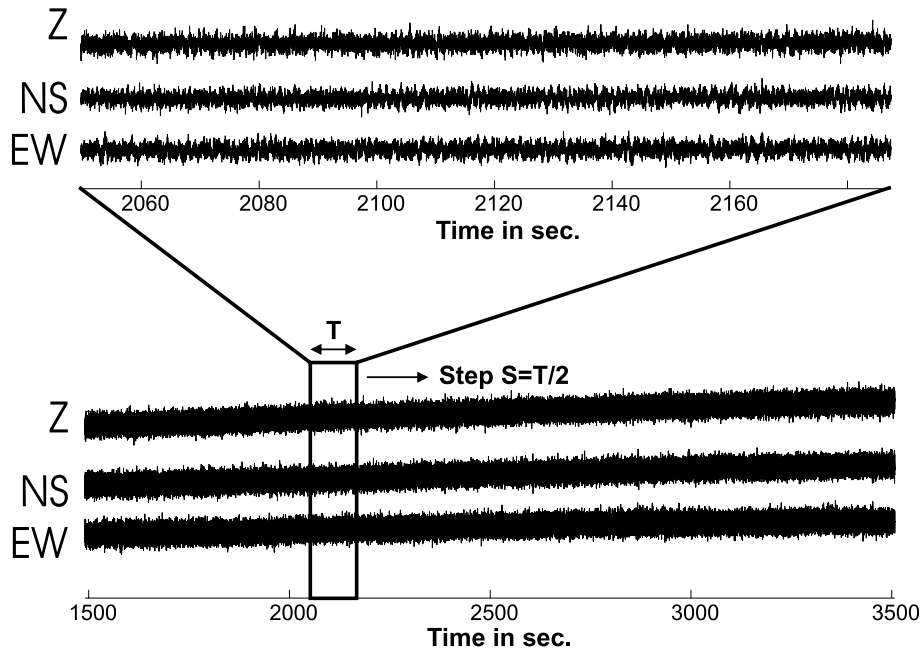
Figure 3. 2000 s sample section analysed (bottom) and T-length moving window processed (top). This noise data set is extracted from station 29A on August 15 at 5 a.m.
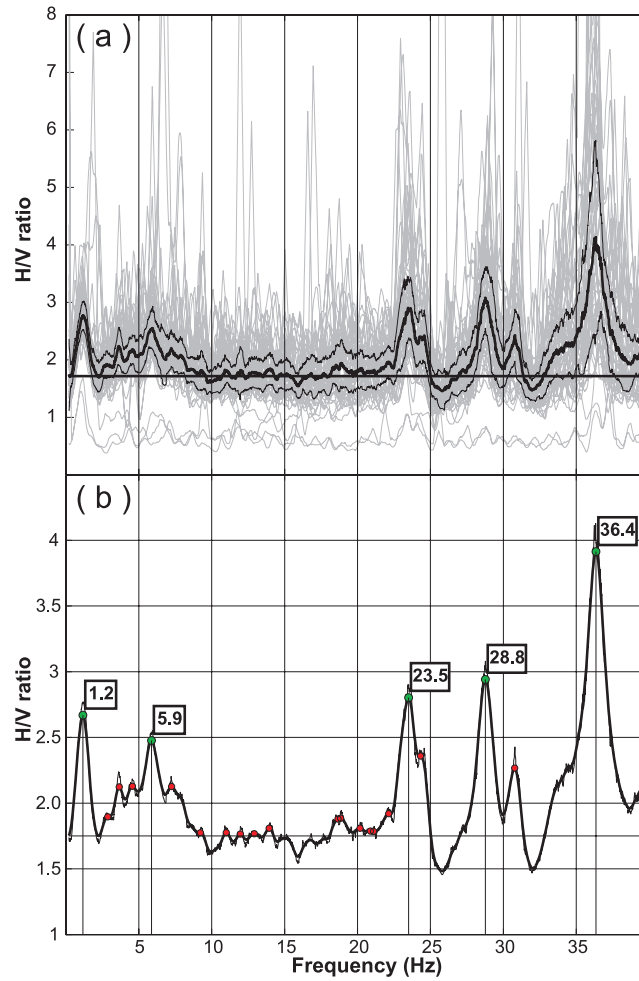
Figure 4. (a) Representation of the whole H/V spectral ratios $r_{i,n}(f)$ of elementary windows at station 29A. The thick bold line depicts the mean value $R_i(f)$ of considered 1-hr time window section. The thin bold lines show the standard deviation of the H/V ratios. (b) Determination of the five main peak frequencies with spectral ratio greater than 1.75.

An example of the obtained N ratios is depicted in Fig. 4a. The mean ratio value $R_i(f)$ (thick bold line) is calculated individually for each frequency, rejecting the ratios amplitudes outside the standard deviation (thin bold line).

$$R_i(f) = L_w \left(\frac{1}{N} \sum_{n=1}^{N} r_{i,n}(f) \right). \tag{2}$$

A maximum of five frequencies per 1-hr section are identified. These frequencies correspond to the most significant peak ratios greater than 1.75 (Fig. 4b). Assuming that each identified frequency f_k may be related to an interface k with a significant impedance contrast, it is related to the mean shear velocity V_k above the interface and to the depth H_k of the interface using the relation

$$f_k = \frac{V_k}{4\,H_k}, \quad \text{where} \quad V_k = \frac{\sum_{j=1}^{k} \beta_j\, h_j}{\sum_{j=1}^{k} h_j} \quad \text{and} \quad H_k = \sum_{j=1}^{k} h_j, \tag{3}$$

where h_j and β_j being the thickness and shear velocity of level j. The higher is the frequency f_k the shallower is the interface (which implies the smaller depth H_k). The resonance frequencies found by the H/V ratio analysis can be interpreted in terms of depths of interfaces.

4.2 Ground motion amplification in composite damaged materials

The ground motion recorded on the rockslide is compared to the measurements taken at the reference site (Field & Jacob 1995; Parolai & Bindi 2004; Parolai *et al.* 2004). The comparison of seismic signals is done between the true ground displacements obtained after deconvolution of the instrumental response (Fig. 2). Ground displacements are analysed in the frequency range 0.1–40 Hz. The reference site is the broadband STS2 station STET provided by the RENASS network and located ≈1 km eastward from the landslide array. The STET is settled on the Iglière rock whose sloping and elevation were similar to those of the rockslide in the area where the array was installed. This set-up allows

to use the STET as a reference station in order to discriminate the amplitude variations induced by steep topography that will be assumed to be similar (Geli *et al.* 1988; Bouchon *et al.* 1996; Bouchon *et al.* 2000; Gaffet *et al.* 2000) to those induced by the rockslide rheology (Price *et al.* 1994; Parolai & Binbi 2004) corresponding to a low velocity zone and by the damaged rockslide superficial materials. Influence of the latter highly fractured superficial soils was related to high frequency amplification (Aster and Shearer 1991a, b; Steidl *et al.* 1996; Moussatov *et al.* 2002; Vlastos *et al.* 2003, 2006).

5 INTEGRATED INTERPRETATION OF THE SEISMIC, GPS AND RAINFALL RECORDS

5.1 H/V spectral analysis

5.1.1 Identification of the rockslide resonance frequencies

Using the H/V method described above (see Section 4.1), the peak resonance frequencies are determined for the stations 29A, 29B, 29C and 29D. They are displayed in Fig. 5. Three main behaviours can be observed:

(1) There are clear alignments of quasi-constant or slowly varying contiguous frequencies with values depending on the station considered.
(2) There are frequencies with sparse alignment or random distribution.
(3) The 1.2-Hz resonance frequency is stable and is observed at all the stations.
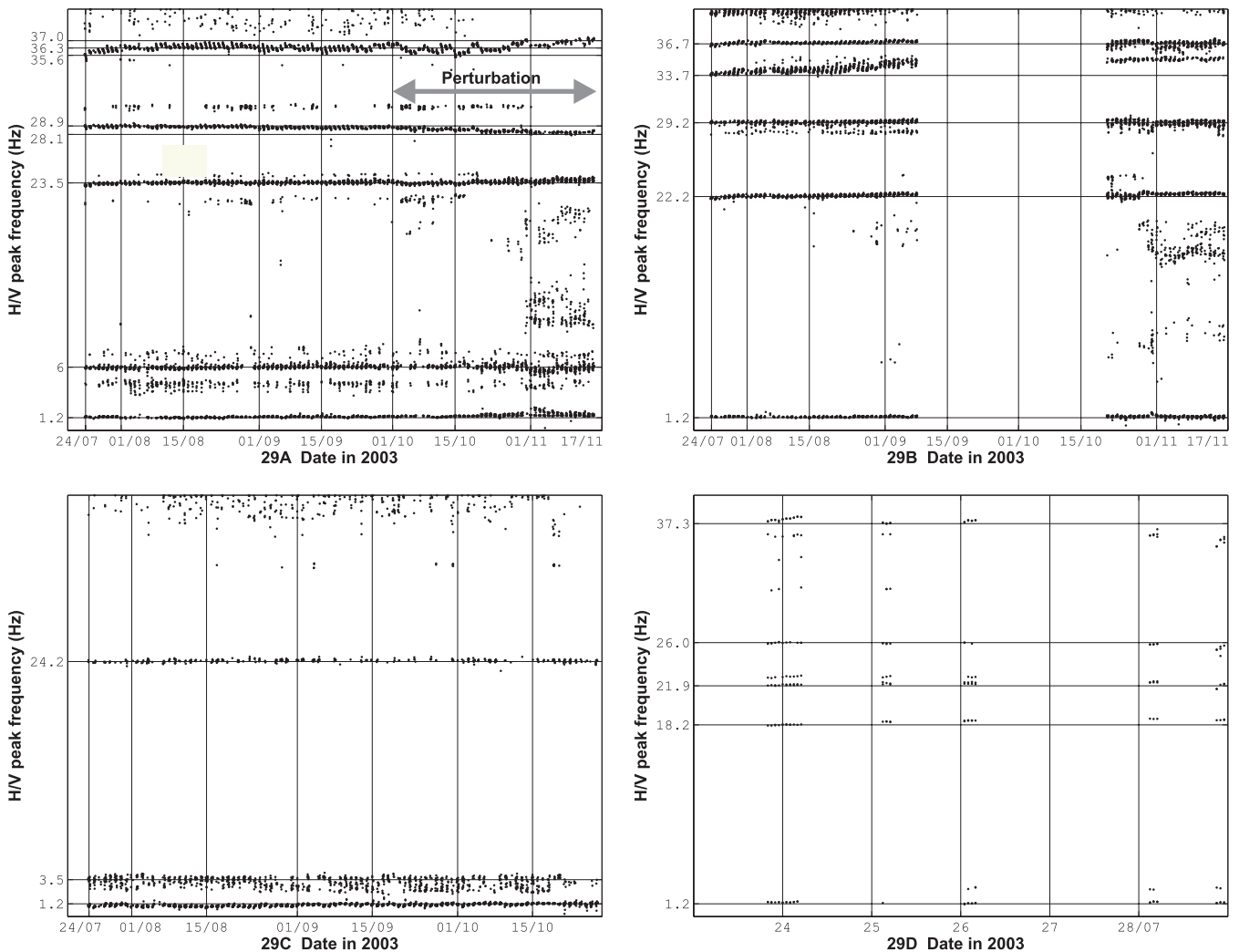
Figure 5. Upper left: resonance frequencies measured by the landslide sensor 29A. Each dot corresponds to a 1-hr-long section of the H/V process. Analysis is focused onto the strong alignments of frequencies annotated along vertical axes, dispersed measurements being interpreted as noise. Upper right: same as (a) for 29B. The lack of data between September and October is caused by the battery-related problem The increase of noise in November at station 29A and 29B is related to a change of sampling rate from 125 to 250 pts s^{-1}. Lower left: same as (a) for 29C. Lower right: same as (a) for 29D. Despite the lack of data due to strong digitizer dysfunctions, the available measurements of resonance frequencies are compatible with the general trend of the other stations.

The 1.2 Hz unvarying low resonance frequency corresponds to the spectral ratio calculated by assuming identical damping factors for both horizontal and vertical components of the used seismometers. The damping factors, determined experimentally, were found to be different, and therefore the associated 1.2 Hz peak is considered to be a metrological artefact and will be excluded from the following discussion.

The frequencies corresponding to the case (2) are interpreted as noise measurements induced by the automatic detection threshold somewhat too sensitive to the analysis method. They will not be considered since they correspond to the peaks with poor detection values that would have been rejected in a handmade analysis.

Thus, only the frequencies corresponding to the case (1) will be interpreted as the rockslide resonance frequencies.

5.1.2 Calibration of frequencies using velocities data from geophysical prospection and geomorphological setting

The results of geophysical prospecting (Jomard *et al.* 2007) performed along the profile *EVR* (see Fig. 1) provide a measurement of apparent *P*-wave velocities on the NE side of the rockslide. Two main velocities are identified in relation with the cohesion, compaction or consolidation of the soil.

(1) A low *P*-wave velocity, $V_P^{\text{uncons.}} = 720 \pm 430 \, \text{ms}^{-1}$ (points EVR4 to EVR8), associated with a shallow layer made up of unconsolidated or weathered soils. The related media is a highly fractured part of the slope.

(2) A high *P*-wave velocity, $V_P^{\text{cons}} = 1970 \pm 230 \, \text{ms}^{-1}$ (points EVR1 to EVR3), associated with a slid and more compacted gneiss which is a major component of the deeper volume of the slope. The medium is a relatively low fractured part of the slope where foliation dips with an angle of $60°$–$75°$ to the north.

The uncertainties of the V_P estimated by Jomard *et al.* (2007) are conservative in the sense that they integrate 100% of the measurement variations (i.e. they can be assimilated to a 2σ error bar). For the rest of the study, the classical σ error bars will be considered, hence $\Delta V_P^{\text{uncons.}} = 215 \, \text{ms}^{-1}$ and $\Delta V_P^{\text{cons.}} = 115 \, \text{ms}^{-1}$.

The standard shear velocity of the superficial soil is assumed to be $V_S^{\text{surf}} = V_P^{\text{uncons.}}/\sqrt{3} \approx 416 \pm 124 \, \text{ms}^{-1}$ (Aki & Richards 1980). If for example the characteristic frequency $f = 24.2 \pm 0.1 \, \text{Hz}$ determined for station 29C, is applied, the associated depth becomes $H^{\text{surf}} \approx 4.3 \pm 1.3 \, \text{m}$. This result means that all frequencies higher than $f = 24 \, \text{Hz}$, found at stations 29A, 29B and 29C, should be related to shallow unconsolidated soils with thicknesses shallower than a few metres.

These shallow soils lay on the second layer mainly identified at stations 29A and 29C by frequencies $f = 3.5 \pm 0.2 \, \text{Hz}$ and $f = 6.0 \pm 0.1 \, \text{Hz}$, respectively. Station 29D also shows a peak frequency around 3–4 Hz but the value cannot be taken into account since it corresponds to very few measurements. None of such low resonance frequency was detected at station 29B.

The shear velocity of the second layer is $V_S^{\text{deep}} = V_P^{\text{cons}}/\sqrt{3} \approx 1137 \pm 66 \, \text{ms}^{-1}$ and the thickness of this second layer is

$$H^{\text{deep}} + H^{\text{surf}} = \frac{V_S^{\text{surf}} \times H^{\text{surf}} + V_S^{\text{deep}} \times H^{\text{deep}}}{4 \times f \times \left(H^{\text{deep}} + H^{\text{surf}}\right)}, \tag{4}$$

which leads to

$$H^{\text{deep}} = \frac{1}{2} \times \left\{ \left(\frac{V_S^{\text{deep}}}{4 \times f} - 2 \times H^{\text{surf}}\right) + \sqrt{\left(\frac{V_S^{\text{deep}}}{4 \times f}\right)^2 - \frac{H^{\text{surf}}}{f} \times \left(V_S^{\text{deep}} - V_S^{\text{surf}}\right)} \right\} \tag{5}$$

The values are reported in Table 1 for the four station sites. The confidence intervals are calculated using the formula

$$\Delta H^{\text{deep}} = \frac{\partial H^{\text{deep}}}{\partial H^{\text{surf}}} \Delta H^{\text{surf}} + \frac{\partial H^{\text{deep}}}{\partial V_S^{\text{surf}}} \Delta V_S^{\text{surf}} + \frac{\partial H^{\text{deep}}}{\partial V_S^{\text{deep}}} \Delta V_S^{\text{deep}} + \frac{\partial H^{\text{deep}}}{\partial f} \Delta f, \tag{6}$$

where $\Delta H^{\text{surf}} = H^{\text{surf}}(\Delta V_S^{\text{surf}}/V_S^{\text{surf}} + \Delta f/f)$, $\Delta V_S^{\text{surf}} = 215 \, \text{ms}^{-1}$, $\Delta V_S^{\text{deep}} = 115 \, \text{ms}^{-1}$, Δf depends on frequency dispersion estimates.

Table 1. Resonance frequencies and related thicknesses at each site.

Sites	f_1 (Hz)	H^{surf} (m)	f_2 (Hz)	H^{deep} (m)	H^{total} (m)
29A	35.6 → 37.0 28.1 → 28.9 23.5 ± 0.1	4.4 ± 1.3	6.0 ± 0.1	40 ± 6	44 ± 8
29B	33.7 → 36.7 29.2 ± 0.2 22.2 ± 0.1	4.7 ± 1.4	None		
29C	24.2 ± 0.1	4.3 ± 1.3	3.5 ± 0.2	74 ± 12	78 ± 14
29D	≈37.3 ?≈ (18.2 → 26.0) ?	≈6 ?	≈(3 → 4) ?	≈60 ?	≈66 ?

Notes: H^{surf} thickness indicates the thicker estimation corresponding to the lower resonance frequency f_1. Results for station 29D should not be regarded as definitive since they were determined from a very short data set.
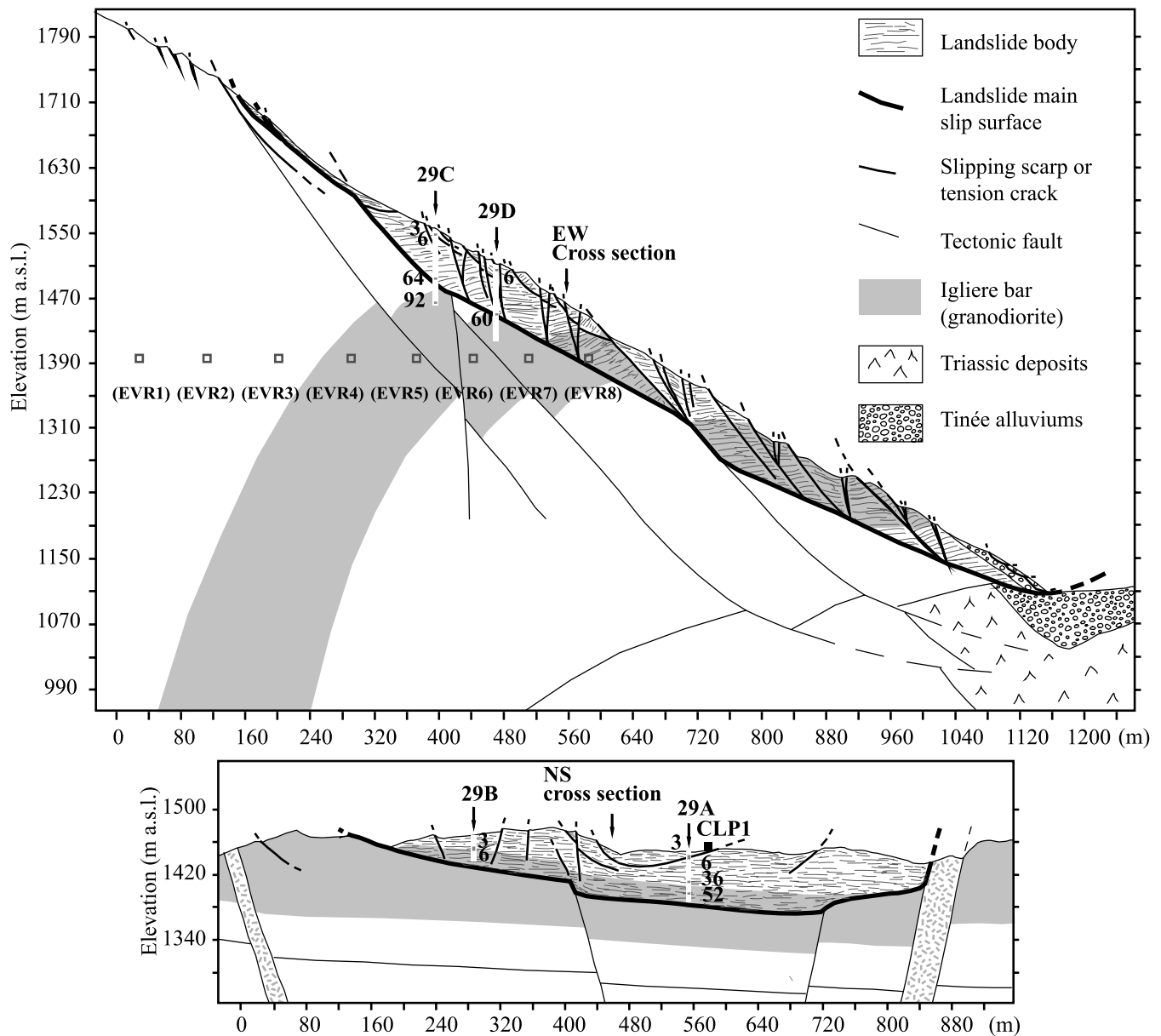
Figure 6. Geological cross-sections of the La Clapière unstable mountain slope. Top: N–S section; bottom: W–E section.

The interval depths H^{surf} and H^{total} are shown in Fig. 6. The calculated deep interface (H^{total}) corresponds well to the case of an interface formed by the highly altered gneisses overlying the low altered granodioritic Iglière bar. The rockslide main slip surface is not clearly identified because it is located within the granodioritic bar. Then, no major velocity contrast has been observed.

The H^{surf} interface is also identified within the gneissic facies. It could be linked to a shallow secondary slip surface that bounds a small destructured landslide imbedded in the main rockslide of the la Clapière. Thus, the contrast between this small block-slide body and the overlying highly fractured cohesive gneisses could explain the identified interface.

At station 29B, the $H^{surf} = [3–6]$ m deep interface can be clearly associated to the same major lithological contrast between altered gneisses and low altered granodiorite. On the NS cross section in Fig. 6, interfaces are identified at depths of $H^{total} = [64–92]$ m and $H^{total} \approx 66$ m at stations 29C and 29D, respectively. Although these depths roughly correspond to the location of the main slip surface, it can be pointed out that, in that area, there is also a strong lithological contrast between the gneissic rockslide body and the granodioritic bar located in the stable zone. At site 29C, the $H^{surf} = [3–6]$ m deep interface is identified and could correspond to the same shallow block-slide as the one at station 29A. This shallow slide is roughly bounded by circular scarps as shown in Fig. 1. Finally, it appears that seismically identified interfaces at relatively great depths correlate better to the strong lithological variations, such as the gneisses/granodiorite contrast, than to the rockslide deformation.

Indeed, at the depth, the strength contrast between the currently moving rockslide body and the stable slope is not so high. However, a high deformation zone is located at the slip surface but it is too thin to be revealed by the method. Closer to the surface and in the case of

Table 2. Main local earthquakes reported by the RENASS seismic agency during the time of the experiment.

Date	Epicentre toponym	Lat. (N)	Long. (E)	Depth (km)	M_L
01/09/2003 19:28	ENE Saint-Sauveur-sur-Tinée (06) Dist. = 39 km (BAZ = N95)	44.22°	7.43°	5	3.4
06/10/2003 12:40	ENE Barcelonnette (04) Dist. = 26 km (BAZ = N328)	44.44°	6.78°	10	2.8

Note: BAZ stands for backazimuth of epicentre. Event locations are plotted in Fig. 1

shallow circular landslide, the slip surface can eventually be identified if the landslide body is highly destructured as compared to the material it is embedded in.

5.1.3 Fluctuation of resonance frequencies

The resonance frequencies, measured at station 29A (upper left, Fig. 5), show fluctuations that started to occur since the beginning of October. The phenomenon appears mainly for the higher resonance frequency alignments with (1) a ±0.7 Hz oscillation around the 36.3 Hz frequency and (2) a decrease of resonance frequency from 28.9 to 28.1 Hz for the second higher frequency. Also, a negligible variation seems to be identifiable around 23.5 Hz. No perturbation can be observed for the lower resonance frequencies. Assuming the shear velocity to be the same for all shallow soils, the roughly approximated depths of each level related to frequencies 36.3 and 28.9 Hz are, respectively, 2.9 ± 0.9 and 3.6 ± 1.1 m. The uncertainty clearly indicates that these interfaces cannot be distinguished from each other although they are identified individually by their resonance frequencies.

The fluctuations of the two higher resonance frequencies may be correlated with the changes in weather conditions. The amount of rainfall increased significantly since the beginning of October. Thus, fluctuating frequency may be attributed to the changes in water saturation of the superficial soils. Water saturation increase leads to a decrease of shear velocity and therefore a decrease of related resonance frequency (eq. 3).

These results show that the groundwater vertical seepage depends on the rockslide body heterogeneous lithology that can be schematically simplified as blocky superficial gneisses, altered gneisses and fractured low altered granodiorite. It can be estimated that blocky superficial gneisses behave like a continuous highly porous layer and that the deep granodiorite behaves like a discontinuous fractured layer. Intermediate altered gneisses could be considered as a double porosity layer. In such a conceptual model, vertical infiltration is widely spreading in the two upper layers where it induces a significant frequency variation while water penetrates only through the fractures at the depth where its location within a small number of fractures does not induces any frequency variation. This vertical hydrogeological contrast induces temporary water storage close to the rockslide surface. However, the observations cannot show incoming water drained from the surface through near vertical fractures and/or groundwater inflows from aquifers in the upper part of the slope and connected to the rockslide. These are the two other groundwater flowpaths considered to be responsible for the rockslide hydrologic recharge (Cappa *et al.* 2004; Guglielmi *et al.* 2005).

5.2 Landslide ground shaking amplification

The rockslide ground motion is studied by using two seismic events of the relatively high magnitude (i.e. Barcelonnette M_L 2.8 and Saint-Sauveur-sur-Tinée M_L 3.4, see Table 2) in order to compare amplitudes at the reference site STET located on the stable slope 1 km northward from the rockslide (STS2 sensor provided by the RENASS network), and at site 29A, located on the rockslide itself (see Fig. 1).
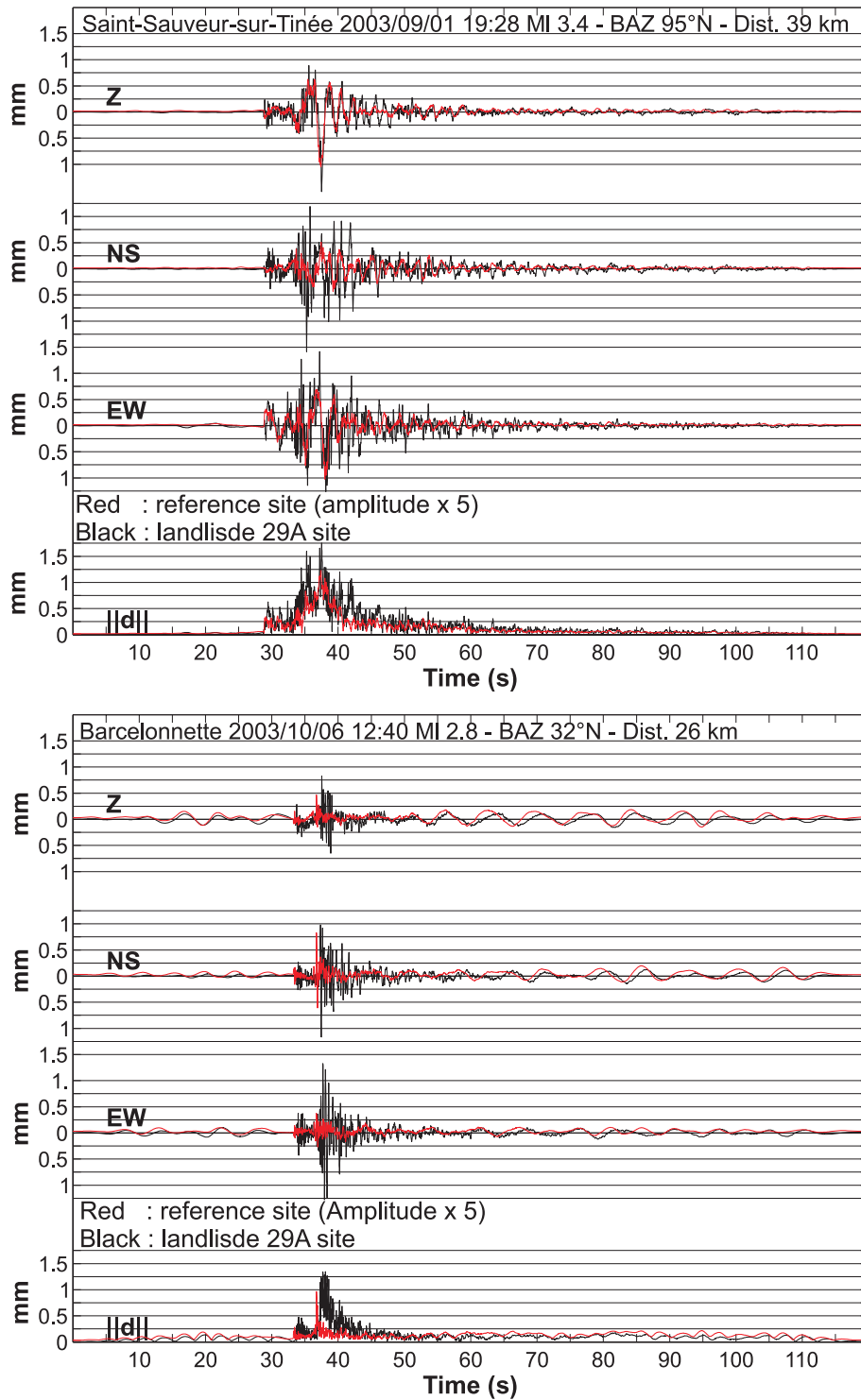
The ground displacement measured on the rockslide in the frequency range [0.1–10 Hz] is superimposed to the measurements done at the reference STET station and shown in Fig. 7. Amplitude of the reference site is multiplied by 5 in order to allow comparison between the stations. Motions are well correlated in the low frequency range. When excited by the Mediterranean meteorological condition, the great amplitude of the Mediterranean swell can maintain quasi-permanent oscillations of the rockslide with important peak-to-peak amplitude of ≈0.25 mm and periods varying between 5 and 7.5 s (Fig. 7, see Barcelonnette earthquake box).

These observations, done in the time domain, are depicted in Fig. 8 in the frequency domain using the mean 0-peak amplitude spectra, defined as

$$S(f) = L_w \left(\frac{2}{T} \sqrt{\left| \int_T z(t)\,e^{-2i\pi ft}dt \right|^2 + \left| \int_T n(t)\,e^{-2i\pi ft}dt \right|^2 + \left| \int_T e(t)\,e^{-2i\pi ft}dt \right|^2} \right), \tag{7}$$

where $z(t)$, $n(t)$ and $e(t)$ are the three components of the ground displacement, T is the time window length, and L_W is the smoothing window. The time window was taken to be 40 s long and centred on the signal.

Spectra in Fig. 8 confirm the ability of the L4C sensors to measure the ground motion in the frequency range from 1 to 0.1 Hz. The Mediterranean Sea swell frequency band is clearly superimposed to the Barcelonnette event. It can be identified on both reference and rockslide sensors with a broad peak centred at ≈6 s period. The non-stable sea swell period implies that the mean 0-peak spectral amplitude is lower than the one measured on the recorded ground motion displayed in Fig. 7. The ground motion spectrum, associated with the Saint-Sauveur-sur-Tinée (M_L 3.4) earthquake, is mainly excited in the frequency range above sea swell (i.e. [0.2–0.7] Hz). For both events, a scaling factor of 5 must be used in order to superimpose the landslide and reference amplitude spectra for frequency below 0.7 Hz.

Figure 7. Ground displacement measured by the broadband STS2 seismometer (in red) at the reference site STET and by the short period L4C seismometer (in black) on the rockslide location 29A, for the two earthquakes (M_L 3.4 and 2.8). The plot displays the Z, NS and EW components of ground displacement. The modulus of displacement ($\|\mathbf{d}\|$) is plotted at the bottom. Amplitude measured at the reference rock site STET is multiplied by 5 in order to be usefully compared to landslide observations.

For frequency above 0.7 Hz, the rockslide recordings show clear amplification in a frequency band that is not specifically excited at the reference site. A strong rockslide amplification effect is thus clearly identified in the corresponding frequency band (roughly above 1 Hz). This high frequency enhancement is not well understood. Since no clear evidence can explain this observation, we emit the hypothesis of a rockslide non-linear effect related to frequency up-conversion induced by wave propagation across the highly damaged area (i.e. the fractured material of the rockslide itself) (Moussatov *et al.* 2002).
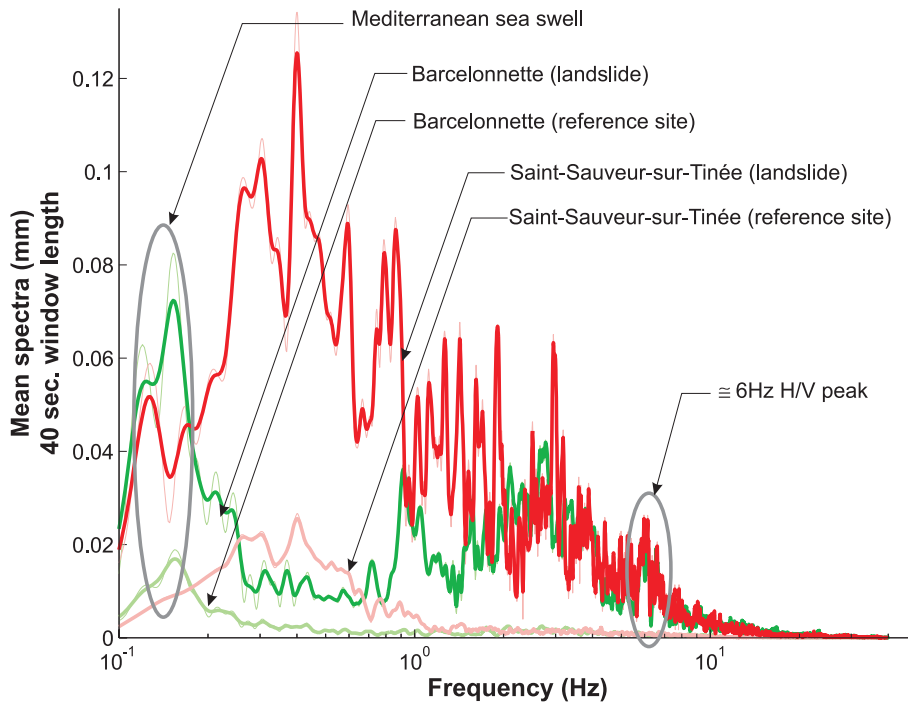
Figure 8. Superposition of mean spectra (eq. 7) of the ground displacement amplitudes measured at the reference site STET (light red and light green solid lines) and at the landslide site 29A (dark red and dark green solid lines). The thin broken red and green lines display the corresponding spectra before smoothing. Sea swell was strong during this period and the corresponding 6 s period is circled with a grey ellipse.
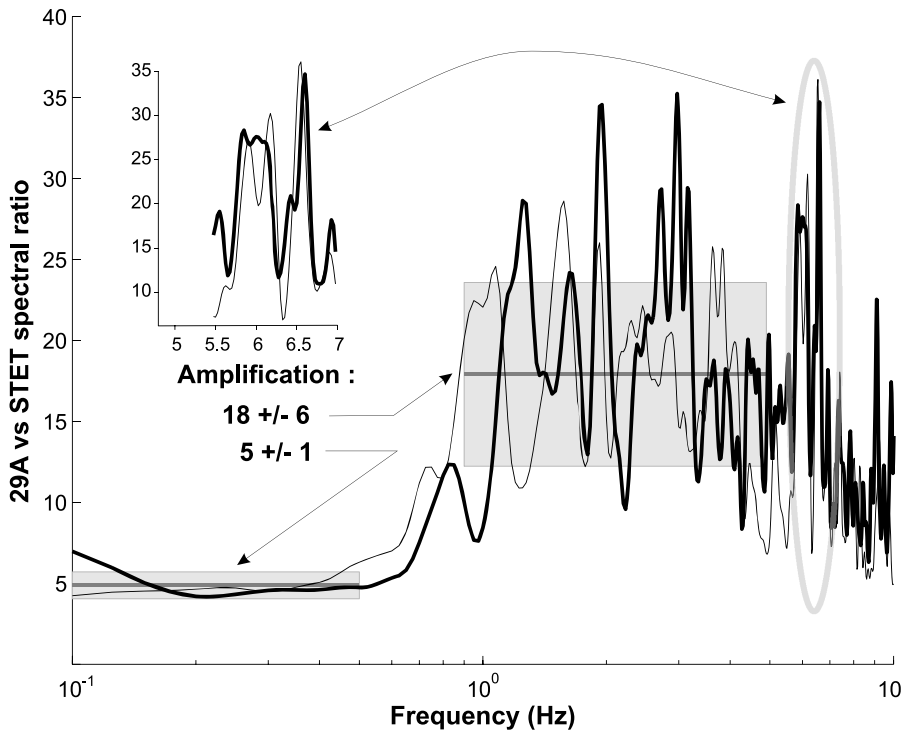
Figure 9. Site versus reference (i.e. 29A versus STET) spectral ratios for ground shakings induced by the Barcelonnette and Saint-Sauveur-sur-Tinée earthquakes.

Two distinct ranges of amplification are thus identified in Fig. 9.

(1) At low frequencies, below 0.7 Hz, the amplification is well constrained with a rate of 5 ± 1.
(2) At high frequencies, above 1 Hz, amplification rate is 18 ± 6. A great variability of the amplification rates is observed but no strong evidence can indicate nonlinear effects between the two events.

Moreover, for both events, double peak amplification is observed around 6 Hz with a remarkably stable ratio. This frequency was also identified using the H/V analysis. The upper left part of Fig. 5 displays a shape similar to that shown in the insert to Fig. 9, associated with this latter double peak: (1) the first broad peak centred around 6 Hz which is the one selected during the H/V analysis; (2) the second thinner peak centred around 6.6 Hz. This thinner peak was also detected by the H/V process but appears sparsely above the broad 6 Hz alignment. Strong amplifications are related to these twin peaks for the two earthquakes, reaching values of 27 and 35 for the broad and thinner peaks respectively.

This analysis shows that the rockslide was strongly shaken during the Saint-Sauveur-sur-Tinée earthquake with a maximum 0-peak instantaneous ground displacement of 1.75 mm (see Fig. 7 for the Saint-Sauveur-sur-Tinée earthquake) and strong vibration with a 0-peak displacement greater than 0.5 mm for a period of time longer than 5 s. These unusual elevated ground displacement values are related to the strong amplification effect identified on the rockslide.

5.3 Long-period rockslide behaviour

5.3.1 Perturbations of slope movements over large timescale observed during continuous GPS monitoring

The GPS motion, depicted in Fig. 10, shows (1) a typical reversible tilt and (2) a change in the rockslide velocity (Fig. 11). This rocking occurred during the period of winter rains, from 2003 October to 2004 February, and may be associated with water filling the failure planes which define the north-eastern border of the block on which CLP1 is settled. Rockslide velocity follows a straight line turned upwards, toward N45 azimuth (upper left box in Fig. 11). This general trend is oblique to the topographic slope orientation that is mainly N–S. It corresponds to a global slowing up period of the rockslide schematically represented by the arrows 1 and 4 in the inset displaying the schematic rockslide behaviour (dashed inset in Fig. 11).

The upper right caption (Fig. 11) shows the projection of the CLP1 velocity in the vertical SW-NE oriented plane. After a continuous rectilinear period of rockslide velocity decrease (inset, arrow 1), it exhibits a period of rockslide speeding up (inset, arrow 2) followed by a slowing down period (inset, arrow 3) before coming back to the general trend of rockslide velocity behaviour (inset, arrow 4). The acceleration is clearly correlated to the fluid flow increase associated with the rainy period.

Considering the projection along a vertical N–S plane oriented along the main topographic slope, the lower left caption shows that the velocity vector remains non parallel to the rockslide topographic slope with a significant horizontal component turned toward the South (see
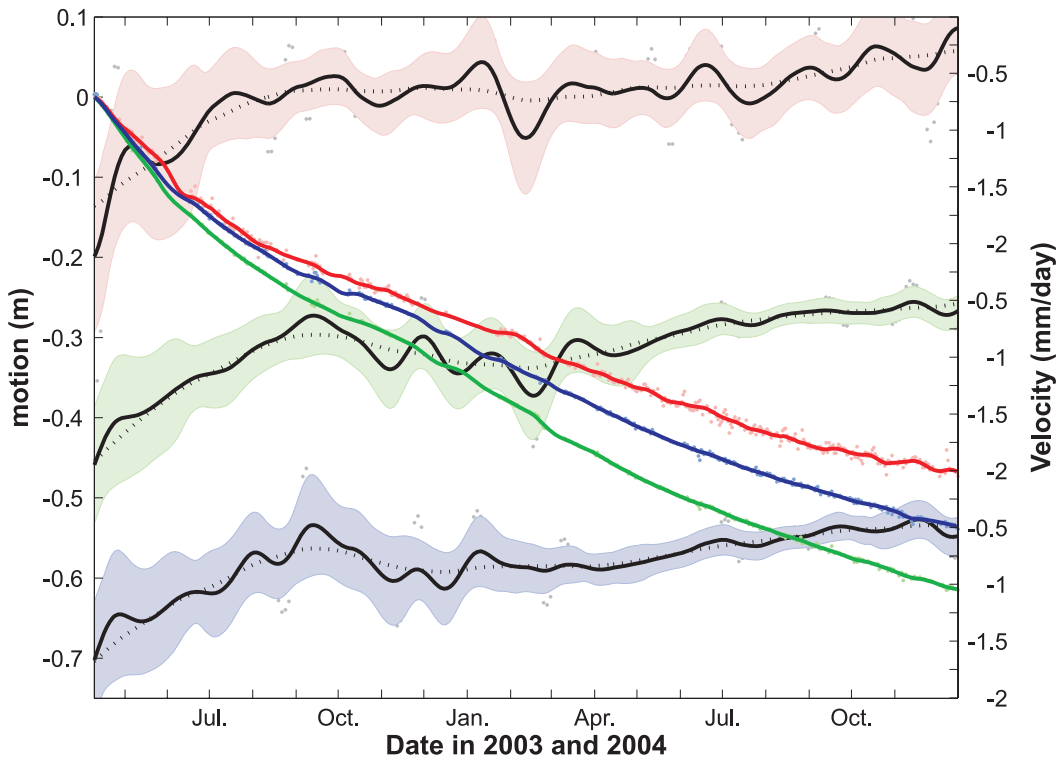
Figure 10. (1) Descending curves show Z (red), NS (green) and EW (blue) ground motion measured by GPS at the location CLP1 (Fig. 1). Dots correspond to the measurements recorded every 30 s, curves show the smoothed motion with a moving window of 2 min (i.e. five points). (2) Ascending curves show ground velocity and standard deviation for the three components Z (red), NS (green) and EW (blue). Grey dots are raw calculation of the smoothed motion curves. The thick bold lines correspond to the smoothed velocity with a moving window of 4 min (10 points); the dashed lines correspond to a moving window of 12 min (30 points).
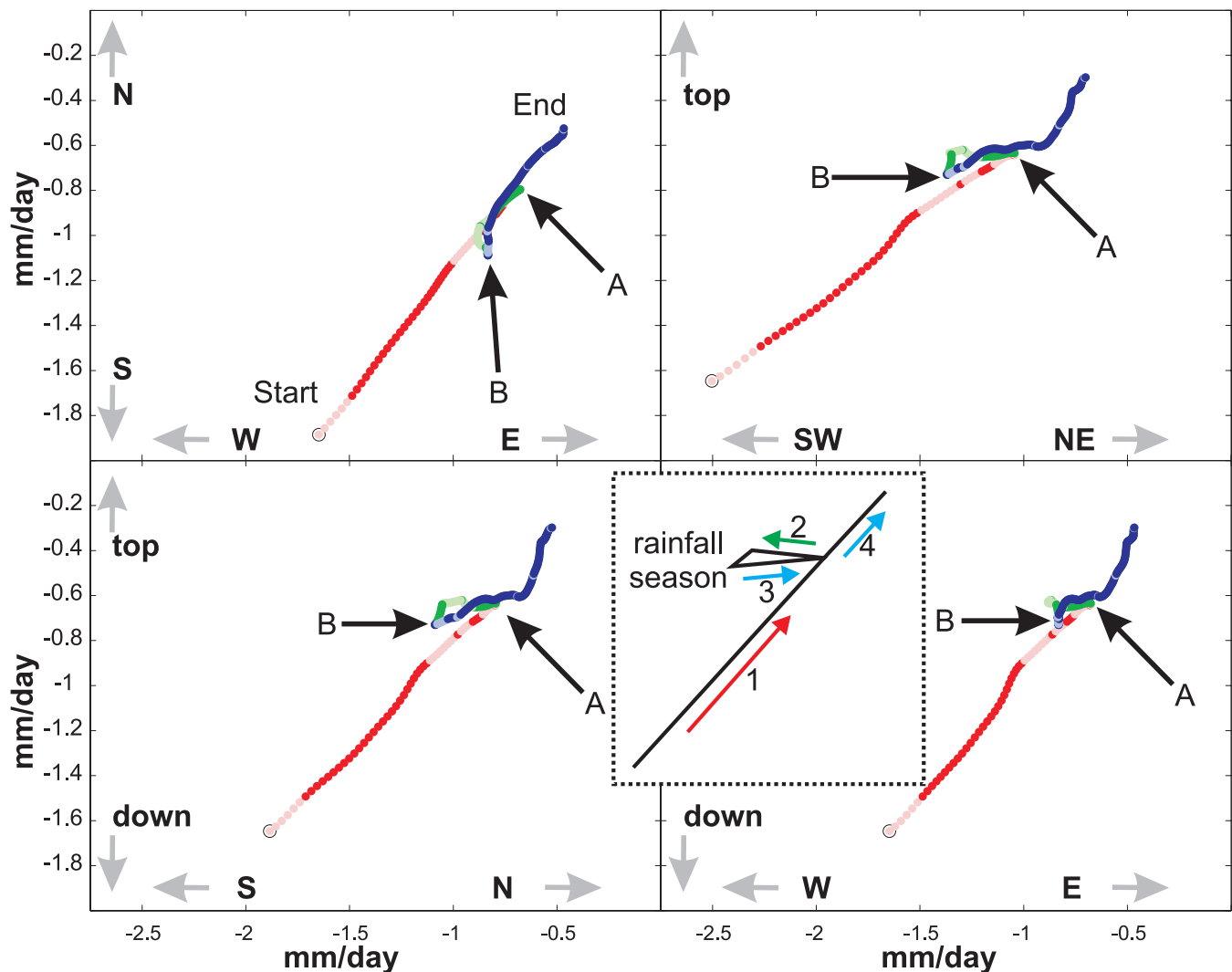
Figure 11. Curves start in 2003 mid-April, end in 2004 December. Turn back points A and B enclose the whole rainy period from 2003 mid-October to the end of 2004 February. Strong colours correspond to real records. Pastel colours correspond to measurements interpolated in ground motions measurements done by GPS and presented in Fig. 10. Inset is commented in the text.

green segment A–B). Correlatively, the lower right caption does not show any significant behaviour for the transverse component of velocity, perpendicular to the topographic slope. This horizontal increase of velocity vector may be interpreted as a downwards rotation (inset, arrow2) followed by an upwards rotation corresponding to an episode of failover and recovery of CLP1 block. At the end of this transitional period of rotation, the rockslide velocity takes again the initial trend characterized by a global slowing up.

6 DISCUSSION

6.1 Interests and limitations of H/V analysis

The microseismic analysis done allowed depth evaluation of strong impedance contrasts that may be associated with (1) strong lithological contrasts and (2) shallow slip surfaces bounding highly destructured circular rockslides. At the depth, such results show that the gravitational deformation of the moving mass remains insufficient to produce a significant impedance contrast as compared to the stable parts of the slope. This proves that in hard rock slopes, rockslide body strengths remain relatively high and that deformation is localized on relatively thin zones that cannot be seen with the indirect microseismic method.

Fluctuations of resonance frequencies are clearly correlated to vertical water seepage. The method allows identification of successive vertical water diffusion through superficial completely destructured rocks down to deep fractured layers. The method is particularly sensitive to water spreading and temporary storage in the shallow destructured layers where water saturation of large volumes could cause weight increase and shallow landslides triggering. It could also be a promising method for an indirect estimation of the amount of water storage near

the rockslide surface. Water drained deeper in the rockslide through the vertical fractures can be responsible with a time delay for the slope movements long after the rainfall happened.

6.2 Site amplification

Two amplification processes control rockslide ground motions. The first one is related to the rheology since wave velocity significantly decreases in the shallowest soils, (i.e. in the rockslide body itself). This rheological site effect generates a frequency-independent amplification by factor of five with respect to the reference consolidated site. The second behaviour concerns the strong amplification measure for high frequency. This amplification related to fracturing of the superficial soils is well identified by Aster & Shearer (1991a, b) and Steidl *et al.* (1996), and may be part of the rockslide attrition. In a similar way, the stationary sea swell shaking of landslide may also be involved in the rockslide stress.

7 CONCLUSION

We have developed a seismic, continuous GPS and meteorological monitoring system and used it to investigate the La Clapière unstable mountain slope in the Southern French Alps. Our sensor network composed of four seismometers, four GPS and three rain gauges was installed over the territory of ∼1.5 km^2 for a period of 4 months. By combining the results of our monitoring system with geological investigations, we can summarize our major findings as follows:

(1) Data analysis allowed us to estimate strong impedance contrasts that may be associated with sliding surface or at least with consolidated part at the base of the sliding body. The depths are related to resonance frequencies clearly identified with the H/V and site to reference spectral ratio techniques. The determined frequencies are sensitive to the amount of the water saturation of the superficial soils. This result means that for the measurement of the characteristic frequency at a given site it is necessary to take into account the fact that water saturation may fluctuate significantly between dry and rainy periods.

(2) Evidences are reported for strong landslide shakings induced by local seismic events. Our study indicated that rockslide ground motion amplifications are related to both the rheology contrast between rockslide body and surrounding consolidated massif and to the fracturing of the shallowest soils that generated high frequency amplification reaching factor greater than 20. Such strong amplification ratio may contribute to superficial landslide attrition.

ACKNOWLEDGMENTS

REFERENCES

Aki, K. & Richards, P.G., 1980. *Quantitative Seismology: Theory and Methods*, W.H. Freeman and Co., New York.

Aster, R. C. & Shearer, P.M., 1991a. High-frequency borehole seismograms recorded in the San Jacinto fault zone, southern California. Part 1. Polarizations, *Bull. seism. Soc. Am.,* **81,** 1057–1080.

Aster, R. C.& Shearer, P.M., 1991b. High-frequency borehole seismograms recorded in the San Jacinto fault zone, southern California. Part 2. Attenuation and site effects, *Bull. seism. Soc. Am.,* **81,** 1081–1100.

Bouchon, M., Schultz, C.A. & Toksöz, M.N., 1996. Effect of three-dimensional topography on seismic motion, *J. geophys. Res.,* **101,** 5835–5846.

Bouchon, M. *et al*. 2000. Evidence for vertical ground accelerations exceeding gravity during the 1997 Umbria-Marche (central Italy) earthquakes, *J. Seism.,* **4,** 517–523.

Bowden, G.B., 2003. Calibration of Geophone Microseismic Sensors—SLAC-TN-05-023 – LCLS-TN-03-6, Department of Energy contract DE-AC02-76SF00515, 9.

Cappa, F., Guglielmi, Y., Merrien-Soukatchoff, V., Mudry, J., Bertrand, C., Charmoille, A., 2004. Hydrochemical modeling of a large moving rock slope interred from slope levelling coupled to spring long-term hydrochemical monitoring: example of the La Clapière landslide (Southern Alps, France), *J. Hydrol.,* **291,** 67–90.

Del Gaudio, V. & Wasowski, J., 2007. Directivity of slope dynamic response to seismic shaking, *Geophys. Res. Lett.,* **34,** L12301, doi:10.1029/2007GL029842.

Deparis, J., Jongmans, D., Cotton, F., Baillet, L., Thouvenot, F. & Dantz, D., 2008. Analysis of rock-fall and rock-fall avalanche seismograms in the French Alps, *Bull. seism. Soc. Am.,* **98**(4),1781–1796, doi:10.1785/0120070082.

CETE Méditerranée, 2002a. Essais d'identification de rupture sismiques sur le glissement de la Clapière (06)—Compte rendu de recherche, Juin 2002.

CETE Méditerranée, 2002b. Utilisation de la méthode H/V bruit de fond sur le glissement de la Clapière (06)—Compte rendu de recherche, Juin 2002.

Eberhardt, E., Spillman, T., Maurer, H.R., Willenberg, T., Loew, S. & Stead, D., 2004. The Randa Rockslide Laboratory: Establishing brittle and ductile instability mechanisms using numerical simulation and microseismicity, in *Proceedings of the 9th International Symposium of Landslides,* pp. 481–487, ed. Balkema, A.A., Brookfield, VT.

Eberhardt, E., Thuro, K. & Luginbuehl, M., 2005. Slope instability mechanisms in dipping interbedded conglomerates and weathered marls—the 1999 Rufi landslide, *Switzerland – Eng. Geol.,* **77,** 35–56.

Field, E.H. & Jacob, K.H., 1995. A comparison and test of various site-response estimation techniques, including three that are not reference-site dependent, *Bull. seism. Soc. Am.,* **85,** 1127–1143.

Finlayson, B. & Statham, I., 1980. *Hillslope Analysis,* Butterworths, London, pp. 230.

Gaffet, S. *et al.* 2000. A site effect study during the 1997 Umbria-Marche (Central Italy) earthquakes, *J. Seism.,* **4,** 525–541.

Geli, L., Bard, P.-Y. & Jullien, B., 1988. The effect of topography on earthquake ground motion: a review and new results, *Bull. seism. Soc. Am.,* **78,** 42–63.

Geertsema, M., Clague, J.J., Schwab, J.W. & Evans, S.G., 2006. An overview of recent large catastrophic landslides in northern British Columbia, Canada, *Eng. Geol.,* **83,** 120–143.

Glade, T., Anderson, M., Crozier, M.J., 2005. *Landslide Hazrd and Risk,* John Wiley, New York.

Gunzburger, Y. & Laumonier, B., 2002. Origine tectonique du pli supportant le glissement de terrain de la Clapière (NW du massif de l'Argentera-Mercantour, Alpes du Sud, France) d'après l'analyse de la fracturation, *C.R. Géosci.,* **334,** 415–422.

Guglielmi, Y. & Cappa, F., 2010. Regional-scale relief evolution and large landslides: Insights from geomechanical analyses in the Tinée Valley (southern French Alps), *Geomorphology,* **177,** 121–129, doi: 10.1016/j.geomorph.2009.11.016.

Guglielmi, Y., Vengeon, J.M., Bertrand, C., Mudry, J., Follacci, J.-P. & Giraud, A., 2002. Hydrogeochemistry: an investigation tool to evaluate infiltration into large moving rock masses (case study of La Clapière and Séchilienne alpine landslides), *Bull. Eng. Geol. Environ.,* **61,** 311–324.

Guglielmi, Y., Cappa, F. & Binet, S., 2005. Coupling between hydrogeology and deformation of mountainous rock slopes: insights from La Clapière area (southern Alps, France), *C. R. Géosci.,* **337,** 1154–1163.

Heincke, B., Maurer, H., Green, G., Willenberg, H., Spillmann, T. & Burlini, L., 2006. Characterizing an unstable mountain slope using shallow 2D and 3D seismic tomography, *Geophysics,* **71,** B241–B256.

Jibson, R.W. & Keefer, D.K., 1992. Analysis of the seismic origin of a landslide in the New Madrid Seismic Zone, *Seismol. Res. Lett.,* **63,** 427–437.

Jibson, R.W. & Keefer, D.K., 1993. Analysis of the seismic origin of landslides: Examples from the New Madrid seismic zone, *Geol. Soc. Am. Bull.,* **105,** 521–536.

Jibson, R.W., Harp, E.L. & Michael, J.A., 1998. A method for producing digital probabilistic seismic landslide hazard maps: an example from the Los Angeles, California, area—U.S, Geological Survey Open-File Report 98-113, 19.

Jomard, H., Lebourg, T., Tric, E., 2007. Identification of the gravitational discontinuity in weathered gneiss by geophysical survey: La Clapière Landslide (France), *Appl. Geophys.,* **62,** 47–57.

Jongmans, D., Hemroulle, P., Demanet, F., Renardy, F. & Vanbrabant, Y., 2000. Application of 2-D electrical and seismic tomography techniques for investigating landslides, *Eur. J. Environ. Eng. Geophys.,* **5,** 75–89.

Jongmans, D. & Garambois, S., 2007. Geophysical investigation of landslides: a review, *Bull. Soc. Geol. Fr.,* **178**(2), 101–112.

Kemeny, J., 2003. The time-dependent reduction of sliding cohesion due to rock bridges along discontinuities: a fracture mechanics approach, *Rock Mech. Rock Eng.,* **36,** 27–38.

Khazai, B. & Sitar, N., 2004. Evaluation of Factors Controlling Earthquake-Induced Landslides Caused by Chi-Chi Earthquake and Comparison with the Northridge and Loma Prieta Events, *Eng. Geol.,* **71,** 79–95.

Mari J.-L., Glangeaud, F. & Coppens, F., 1997. Traitement du signal, *Ed. Technip,* 460.

Meric, O., Garambois, S., Jongmans, D., Wathelet, M., Chatelain, L. & Vengeon, J.M., 2005. Application of geophysical methods for the investigation of the large gravitational mass movement of Séchilienne, France, *Can. Geotech. J.,* **42,** 1105–1115.

Meric, O., Garambois, S., Malet, J.P., Cadet, H., Guéguen, P. & Jongmans, D., 2007. Seismic noise-based methods for soft-rock landslide characterization, *Bull. Soc. Geol. Fr.,* **178**(2), 137–148.

Moussatov, A., Castagnède, B. & Gusev, V., 2002. Frequency up-conversion and frequency down-conversion of acoustic waves in damaged materials, *Phys. Lett. A,* **301,** 281–290.

Nakamura, Y., 1989. A method for dynamic characteristics estimation of subsurface using microtremors on the ground surface, *Quater. Rep. Railway Tech. Res. Inst. Japan,* **30,** 25–30.

Nakamura, Y., 2000. Clear identification of fundamental idea of Nakamura's technique and its applications, in *Proceedings of the XII World Conference, Earthquake Engineering,* New Zealand paper no. 2656, pp. 8.

Noverraz, F., Bonnard, C., Dupraz, H. & Huguenin, L., 1998. Grands glissements de versants et climat-VERSINCLIM-Comportement passé, présent et futur des grands versants instables subactifs en fonction de l'évolution climatique, et évolution en continu des mouvements en profondeur – Rapport final PNR 31, vdf Hochschulverlag AG an der ETH Zürich, 314.

Nogoshi, M. & Igarashi, T., 1970. On the propagation characteristics of microtremors, *J. Seism. Soc. Jpn.,* **23,** 264–280.

Parolai, S. & Bindi, D., 2004. Influence of soil layer properties on k evaluation, *Bull. seism. Soc. of Am.,* **1,** 349–356.

Parolai, S., Bindi, D., Baumbach, M., Grosser, H., Milkereit, C., Karakisa, S. & Zünbül, S., 2004. Comparison of different site response estimation techniques using aftershocks of the 1999 Izmit earthquake, *Bull. seism Soc. Am.,* **94,** 1096–1108.

Price, R.H., Martin III, R.J. & Haupt, R.W., 1994. The Effect of Frequency on Young's Modulus and Seismic Wave Attenuation – Sandia National Laboratory report SAND92-0847 Distribution, Unlimited Release Category UC-814, 66.

Scavia, C., 1995. A method for the study of crack propagation in rock structures, *Géotechnique,* **45,** 447–463.

Spillman, T., Maurer, H.R., Willenberg, H., Evans, F.E, Heincke & Green, A.G., 2007a. Characterization of an unstable rock mass based on borehole logs and diverse borehole radar data, *J. appl. Geophys.,* **61,** 16–38.

Spillman, T., Maurer, H., Green, A.G., Heincke, B., Willenberg, H. & Husen, S., 2007b. Microseismic investigation of an unstable mountain slope in the Swiss Alps, *J. geophys. Res.,* **112,** B07301, doi:10.1029/2006JB004723.

Steidl, J. H., Tumarkin, A.G. & Archuleta, R., 1996. What is a reference site?, *Bull. seism. Soc. Am.,* **86,** 1733–1748.

Vlastos, S., Liu, E., Main, I.G. & Li, X.-Y., 2003. Numerical simulation of wave propagation in media with discrete distributions of fractures: effects of fracture sizes and spatial distributions, *Geophys. J. Int.,* **152,** 649–668.

Vlastos, S., Liu, E., Main, I.G., Schoenberg, M., Narteau, C., Li, X. Y. & Maillot, B., 2006. Dual simulations of fluid flow and seismic wave propagation in a fractured network: effects of pore pressure on seismic signature, *Geophys. J. Int.,* **166,** 825–838.

Wilson, R.C. & Keefer, D.K., 1983. Dynamic analysis of a slope failure from the 6 August 1979 Coyote Lake, California, earthquake, *Bull. seism. Soc. Am.,* **73,** 863–877.